Environmental Research 204 (2022) 111978

Contents lists available at ScienceDirect

Environmental Research

journal homepage: www.elsevier.com/locate/envres

Ground-based remote sensing of CH_4 and N_2O fluxes from a wastewater treatment plant and nearby biogas production with discoveries of unexpected sources

Magnus Gålfalk [a,*], Sören Nilsson Påledal [b], Robert Sehlén [b], David Bastviken [a]

[a] Department of Thematic Studies – Environmental Change, Linköping University, 581 83, Linköping, Sweden
[b] Tekniska Verken i Linköping AB, Box 1500, 581 15, Linköping, Sweden

ARTICLE INFO

Keywords:
Methane
Nitrous oxide
Wastewater treatment
Biogas production
Hyperspectral imaging

ABSTRACT

This study is an attempt to assess CH_4 and N_2O emissions from all the treatment steps of a wastewater treatment plant (WWTP) in Sweden, serving 145 000 persons, and an adjacent biogas production facility. We have used novel mid-IR ground-based remote sensing with a hyperspectral camera to visualize and quantify the emissions on 21 days during a year, with resulting yearly fluxes of 90.4 ± 4.3 tonne CH_4/yr and 10.9 ± 1.3 tonne N_2O/yr for the entire plant. The most highly emitting CH_4 source was found to be sludge storage, which is seldom included in literature as in-situ methods are not suitable for measuring emissions extended over large surfaces, still contributing 90 % to the total CH_4 emission in our case. The dominating N_2O source was found to be a Stable High rate Ammonia Removal Over Nitrite reactor, contributing 89 % to the total N_2O emissions. We also discovered several unexpected CH_4 sources. Incomplete flaring of CH_4 gave fluxes of at least 30 kg CH_4/min, corresponding to plume concentrations of 2.5 %. Such highly episodic fluxes could double the plant-wide yearly emissions if they occur 2 days per year. From a distance of 250 m we found a leak in the biogas production facility, corresponding to 1.1 % of the CH_4 produced, and that loading of organic material onto trucks from a biofertilizer storage tank contributed with high emissions during loading events. These results indicate that WWTP emissions globally may have been grossly underestimated and that it is essential to have effective methods that can measure all types of fluxes, and discover new potential sources, in order to make adequate priorities and to take effective actions to mitigate greenhouse gas emissions from WWTPs.

1. Introduction

During wastewater treatment, the greenhouse gases (GHGs) methane (CH_4), nitrous oxide (N_2O), and carbon dioxide (CO_2) are emitted to the atmosphere (Hofman et al., 2011). Large emissions of CH_4 and N_2O, which are present in high amounts in wastewater, can have a significant impact on global warming as the 100-year global warming potentials of CH_4 and N_2O are 34 and 265 times higher than CO_2 (Myhre et al., 2013).

The waste and wastewater industry contributes approximately 3 % of the global anthropogenic emissions of GHGs (IPCC 2007), with the landfills and waste sector together making up about 68 Tg CH_4 yr^{-1}, or 12 % of total global anthropogenic emissions (Saunois et al., 2020). Wastewater with its high organic content is treated anaerobically. This is turn leads to increased CH_4 emissions, and with an excessive and rapid urban development worldwide higher future CH_4 emissions are expected unless appropriate mitigation policies are designed and implemented rapidly (Saunois et al., 2020).

Currently the most frequently used methods for estimating GHG emissions at wastewater treatment plants (WWTPs) are in-situ methods such as flux chamber or point source emission measurements at locations where such approaches are possible, and sample collection, bringing sludge material to a lab for follow-up measurements and incubation experiments. Tumendelger et al. (2019) used flux chambers to measure the CH_4 and N_2O emission rates from different treatment steps having air-water interfaces in two municipal WWTPs in Germany. Willén et al. (2016) stored dewatered digested sewage sludge in meter-sized cylinders and measured CH_4 and N_2O during a year, testing the effect of different environmental conditions and addition of

* Corresponding author.
E-mail addresses: magnus.galfalk@liu.se (M. Gålfalk), Soren.Nilsson-Paledal@tekniskaverken.se (S.N. Påledal), Robert.Sehlen@tekniskaverken.se (R. Sehlén), david.bastviken@liu.se (D. Bastviken).

https://doi.org/10.1016/j.envres.2021.111978
Received 14 May 2021; Received in revised form 19 August 2021; Accepted 24 August 2021
Available online 2 September 2021

ammonia to reduce emissions.

A treatment step that could potentially have very high CH_4 emissions, but is more difficult to measure using in-situ methods, is dewatered sludge storage, produced after the digestion of wastewater in large digestion chambers. The difficulty arise as sludge storage takes up a very large surface area, which flux chambers cannot sample in a representative way, and active gas production in the sludge can continue during the storage time before being used in agriculture. A similar situation is open digestate storage tanks at biogas production plants. Scheutz and Fredenslund (2019) measured fluxes from 23 biogas plants using a tracer gas dispersion method and found CH_4 losses in the range 0.4–14.9 % from biogas production, with wastewater treatment biogas plants having the highest losses (7.5 % in average) and open storage tanks being the dominant source.

Remote sensing of GHGs uses infrared (IR) radiation to detect and quantify emissions from a distance, having several advantages over in-situ methods such as not disturbing everyday operations at an industrial site and being able to cover a large area in a short time. Examples from literature include CH_4 mapping of natural gas fields from an airplane (Thorpe et al., 2016) at about 1 m resolution, and the upcoming MethaneSat satellite targeting emissions from oil and gas operations, typically within an area of 200 × 140 km^2, with a similar instrument, MethaneAir, already tested successfully on airplanes (Staebell et al., 2021). While satellites have provided a major progress in global overviews of GHGs, their spatial resolutions have typically been >10 km/pixel (e.g. Bril et al., 2013), hampering source identification. Recently, however, satellites have been launched targeting high emission point sources at much higher resolutions, such as GHGSat-D with a 50 m resolution within a 12 km^2 area (Jervis et al., 2021). The upcoming MethaneSat targets emissions from oil and gas operations within an area of 200 × 140 km^2, with a similar instrument MethaneAIR having been tested successfully on airplanes (Staebell et al., 2021).

Ground-based remote sensing has both high spatial resolution and high sensitivity as its advantages as longer measurement times and shorter target distances are used. An example is hyperspectral quantification of CH_4 and N_2O emissions from waste incineration (Gålfalk and Bastviken, 2018) and CH_4 flux measurements from a refinery using an active (DIAL) system mounted on a truck (Chambers and Strosher, 2008). Ground-based remote sensing has the capacity to map different emission sources at a WWTP, with the ability to find unknown sources that can be quantified in post-processing, and to include all the treatment steps of a plant. In this study we have measured CH_4 and N_2O emissions from all eleven treatment steps at the Linköping WWTP in Sweden using a hyperspectral camera technique. Emission estimates also include emissions from a connected biogas plant, with several previously unknown emissions sources found at both plants. To our knowledge this type of ground-based remote sensing has not been applied previously in WWTPs, where it could be of high importance as many potential fluxes are challenging to reliably estimate using traditional methods.

2. Data and methods

This study presents a one-year study visualizing and quantifying CH_4 and N_2O emissions from all the process steps at a WWTP in Linköping, Sweden based on 21 measurement days in 2018–2019 covering all four seasons. To investigate temporal variability in emissions on short (days/weeks) to long (seasons) time scales, we aimed for five measurement days in each season. CH_4 and N_2O emissions from all the process steps at the WWTP (Fig. 1) were visualized and quantified using ground-based remote sensing from distances in the range 10–250 m. Our measurements also aimed at including potential CH_4 emissions from an adjacent biogas plant.

The Linköping WWTP receives about 42 000 m^3 of wastewater each day, with 145 000 people connected, and includes treatment steps that are mechanical, chemical, and biological, with the water having a residence time of around 12 h at the plant before reaching the small river Stångån.

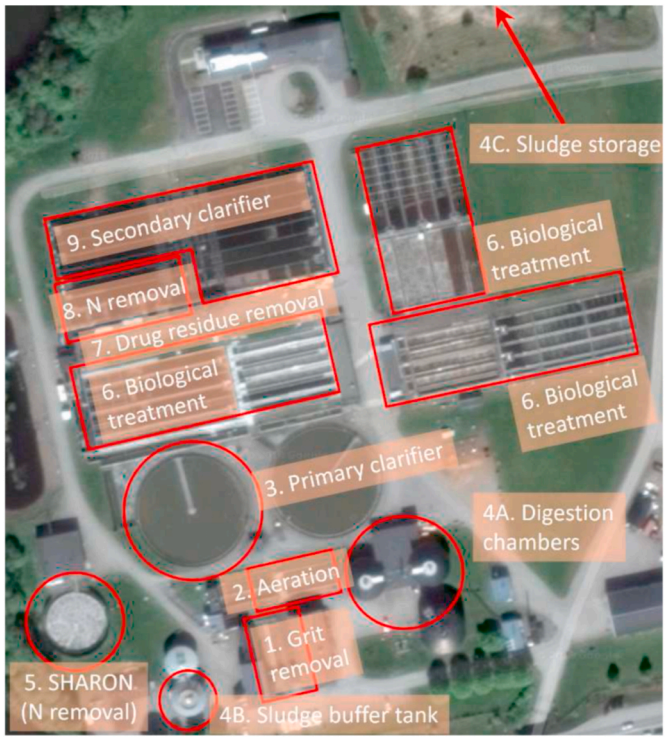

Fig. 1. An overview of the process steps at the Linköping WWTP.

2.1. Hyperspectral camera and other equipment

We have used a customized mid-IR hyperspectral camera (Telops HyperCam Methane), sensitive in a narrow spectral range that includes the highly absorbing 7.7 μm band of CH_4 and the double band of N_2O in the range 7.57–8.07 μm as well as spectral features of H_2O. The system (described in Gålfalk et al., 2016) has since then been complemented with a customized Lidar (DST Control AB) that simultaneously maps background distances in the same field of view as the camera (25 × 20 deg). The spectral resolution (which is variable and can be set to values > 0.25 cm^{-1}) was set to 1 cm^{-1} in this project, which we found to be a good compromise in our spectroscopic modeling between separating spectral features of different species (CH_4, N_2O, and H_2O) and the total exposure time. As the hyperspectral camera is an imaging Fourier transform spectrometer, each measurement consists of a so-called data cube (typically generated over 15–60 s), with an interferogram for each pixel on the detector (up to 320 × 256 pixels).

The camera (weight about 30 kg) is set up on a tripod, having the Lidar mounted on top, and connected to a field computer typically located on a foldable table. The Lidar runs on a battery, but the camera and computer was connected to a power outlet at the WWTP in most of the cases. For the sludge deposits, located on a field far from any buildings, we used a Honda eu30i electrical generator running on petrol which was located at least 25 m downwind from the camera. An overview of the instrumentation is shown in the Supplementary data. Each field of view, or scene, consisted of many data cubes (often at least 16, but more in case of known low emissions) in order to achieve a lower detection limit. Advantages with the method are that unknown emissions anywhere in a scene can be detected and quantified in post-processing, the ability to measure several species at once, not disturbing everyday activities at a plant as everything is measured from a distance (up to hundreds of meters), and that interference-corrected videos can be made from the interferograms for visualization and calculation of

air movement – in turn meaning that flux calculations can be made from the combined concentration and air transport mapping. Disadvantages are that a temperature contrast (of at least 1 °C) is needed between the background and gas temperatures, in order to achieve sufficient absorption or emission lines for quantifying the gas content, which means that the sensitivity of the method is weather dependent. The performance of the camera system and of the flux calculation approaches have been carefully evaluated under various conditions as reported elsewhere (Gålfalk et al. 2016, 2017; Gålfalk et al. 2018) in different types of environments and for controlled gas emissions, comparing results with a portable CH4 analyzer (the Los Gatis Inc. UGGA instrument) and syringe samples analyzed by gas chromatography. As the method relies on absorption spectroscopy, without any additional instruments needed, it uses less assumptions than traditional methods (e.g. flux chambers) and is less influenced by potentially confounding factors such as disturbing the sampled area, sample procedures, sample storage, lab analyses, possible leakage, materials interacting with gases, temperature and pressure changes.

We also used a portable Vaisala WXT520 weather station for many of the measurements, as a complement to the gas speeds calculated from the hyperspectral data. This was done for two reasons: as a backup in case there was low temperature contrast in the remote sensing data and as a control to compare gas transport velocities.

2.2. Spectroscopic modeling (quantification)

The spectroscopic modeling (see Gålfalk et al., 2017 for details) is based on simultaneous fitting of CH_4, N_2O and H_2O in selected spectral windows where these species have strong absorption bands. This is done for each pixel in a scene, meaning that there could be up to 320 × 256 model solutions made to produce gas concentration maps.

Large look-up tables are used in Matlab, containing pre-calculated models of transmission curves (1024 curves for each species; each step corresponding to about 1 m increase in ambient air and using the instrument profile and resolution of the measurements) in order to speed up the calculations considerably. For each pixel, initial models are made for three very different column densities (ppm·m) for all three species (meaning a grid of 3 × 3 × 3 = 27 models) e.g. 0, 500 and 1000 ppm m for CH_4. The model with the smallest residuals in this grid of models is chosen as the center point for the next iteration, with a new smaller grid of 3 × 3 × 3 models centered on this column density. This continues until the grid of models is small enough to only use adjacent transmission curves in the lookup-tables, where an interpolation is made for the final best-fit model. Pixel-by-pixel this technique is used to render column density maps of CH_4, N_2O and H_2O. The models are often divided into layers, also including parameters such as air temperature (from the most highly absorbing H_2O lines), background temperature (from the spectral continuum), and background emissivity (estimated using reflected sky spectra) in cases with high reflectivity; all which can be visualized after the rendering of a scene into maps.

2.3. Air motion modeling

The same interferograms that are used to calculate spectra can also be corrected for interference and visualized as a large set of images or made into a video. The signal will be dominated by the thermal heat radiation from the background, but by subtracting two frames made with a slight difference in time only the signals that change are kept. Adding many such difference images (e.g. subtracting 20 frames taken at time t = 0.40–0.54 s from 20 frames at times t = 0–0.14s) the S/N can be greatly improved. This results in a video of scene changes (mostly gas motion but also flying birds, moving cars etc.) consisting of more than 3500 frames if a spectral resolution of 1 cm^{-1} is used, corresponding to the same time-period as the spectra used for the gas concentrations maps.

Feature tracking of gas structures in a video yields gas speed and direction from autocorrelation of identified emissions, as we have a corresponding distance map of the scene from the Lidar and the time step between frames is known. In case of very weak signal (low temperature contrast) or to get values for gas extended over large areas, simultaneous measurements from the weather station at some distance from the source can be used to verify air motion. The advantage with hyperspectral air motion tracking, which was preferentially used, is that it gives the average air speed close to an emission source.

2.4. Flux calculations

By combining the column density maps, calculated air motion, and known geometry from distance mapping, the emission from a point source or extended source can be calculated for both CH_4 and N_2O (see Gålfalk and Bastviken, 2018 for an example involving waste incineration). The camera was, whenever possible, set up perpendicular to the wind direction and outflows from a source were calculated across a vertical area (vertical line with column densities in the gas maps just downwind of a source); this outflow is subtracted from the inflow (obtained from a similar vertical line upwind of a source) to obtain the emission. In the case of vertical air motion, a horizontal area is used for the mass balance calculation. Averaged emissions can be calculated from a single cube in case of high emissions (typically over times of 15–60 s depending on the spectral resolution and the detector area used), resolving emission changes between cubes with high temporal resolution, or in the case of low emissions, using many averaged cubes for each emissions estimate.

The detection limit of the system is dependent on the background – gas temperature contrast, the number of averaged cubes for a scene, and the background and gas distances. For a temperature difference of 1 °C (it is often much higher in sunny conditions), a background distance of 50 m, and using 16 cubes for each scene (the minimum used in this study) the detection limit for CH_4 is about 65 ppm m, but it can be as low as a few ppm·m if many averages are used and for a temperature contrast of about 10 °C (Gålfalk et al., 2017). In terms of real-world emission detection limits, this will also depend on factors such as wind speed, the geometrical gas distribution, and the scene background (with water being a very reflective background except for when it is seen from angles close to the surface normal). For the conditions and the methods used in this study we detected extended emissions down to 0.3 kg N_2O/d, which can also be considered a conservative detection limit for CH_4 (as the method is much more sensitive for CH_4 than N_2O due to more defined absorption features in the spectra) for the emissions detected in this study.

3. Results and discussion

The results include emissions both from expected and previously unknown sources, for CH_4 and N_2O at the WWTP and the nearby biogas plant, described and discussed in separate sections below.

3.1. Wastewater treatment plant

Treatment steps will be presented in the same order as in Table 1, with an estimate of the total WTTP emission in the last section.

3.1.1. Grit removal

Modeling of this scene was based on at least 16 hyperspectral cubes for each of the two parallel grit removal steps, each giving a CH_4 distribution map (Fig. 2). It is clear that higher gas concentrations were found in regions with slow moving air (being in wind shadow).

The spectroscopic modeling included measurements of the clear sky including its reflections off of the far wall, producing column densities of H_2O, CH_4, and N_2O for all pixels in the scene. We calculated total CH_4 emissions from mass balance calculations using the far wall as a thermal background, measuring vertical air motion from movement of water

Table 1
Treatment steps at the Linköping WWTP. Numbers, which are also marked in the overview (Fig. 1), refers to their order relative to the water and material transport through the plant.

No.	Description of process step
1	In the grit removal, sand and gravel is removed. Iron sulphate is added to increase the separation of phosphorus and organic material from the wastewater.
2	The aeration step mixes the wastewater to reduce odor and to distribute the added iron sulphate more evenly.
3	Two circular pre-sedimentation basins where the formed flocks settle.
4A	The sedimented material (from 3) is pumped into three digestion chambers where sludge is digested in anaerobic conditions at a mesophilic temperature (38 °C) for 20 days. Produced gas (≈65 % CH_4 and ≈35 % CO_2) is transported via a pipeline to an adjacent biogas plant (800 m north) for upgrading to 97 % CH_4 to be used in vehicles.
4B	Residual sludge (from 4A) is stored for 1–3 days in a buffer tank.
4C	After dewatering using a screw presses, the sludge is stored for at least 6 months in a sludge pile, with a new pile made for each calendar month.
5	The reject water from the dewatering process is quite rich in ammonia and is treated in a process called Stable High rate Ammonia Removal Over Nitrite (SHARON) which involves an open basin with a continuous flow of water from the dewatering of sludge (4B) used for removal of ammonia. This step has a 90 min cycle of alternating nitrification (oxic, aeration) and denitrification (anoxic, non-aeration) periods. The length of the oxic period is dependent on water inflow and ammonium content and dosing ethanol as a carbon source takes place at the beginning of the non-aeration period. Nitrification is the biological oxidation of ammonia to nitrite/nitrate. N_2O can be produced in the during the reduction of nitrate/nitrite in anaerobic conditions. After this process the water is pumped back to the grit removal stage (1).
6	The liquid part from pre-sedimentation (3) is pumped to aerated basins where microorganisms break down organic material. Organic nitrogen is converted to ammonia and nitrate (NH_4-N and NO_3-N). This biological treatment stage has periods with and without aeration, with durations that are determined by the nitrogen content of the ammonium and nitrate (NH_4-N, NO_3-N).
7	Ozone is added to break down drug residues (≈90 % is removed).
8	The last step for nitrogen removal uses a Moving Bed Biofilm Reactor (MBBR), with a carbon source added for growth of microorganisms. Here dissolved nitrogen is converted to nitrogen gas.
9	In the after-sedimentation basins aluminum chloride is added to further reduce phosphorus material.

vapor patterns in the IR videos across the horizontal area marked with a white line in panel B of Fig. 2, and combining this with CH_4 column densities along this line. Average yearly emissions based on our four measurements (one for each season) in the ranges 2.4–17 kg CH_4/d and 0–3.7 kg N_2O/d were calculated to 3160 ± 1250 kg CH_4 and 360 ± 330 kg N_2O, respectively.

3.1.2. Aeration

The aeration process step was measured three times (autumn, spring, summer) using a wall, heated by the Sun, as a background. The yearly CH_4 emission, based on measurements in the range 1.5–4.2 kg CH_4/d, was found to be 960 ± 290 kg CH_4, with no N_2O emissions detected. Air motion was calculated from the hyperspectral data cubes.

3.1.3. Primary clarifier

Despite six attempts (over three seasons) to find elevated CH_4 or N_2O levels from the primary clarifier we did not detect any emissions from this treatment step, suggesting that fluxes were low relative to the emitting surface and the air masses passing the tanks during the measurement period (diluting the emitted gas). Hence, this treatment step contributed negligible emissions compared to total emission from the WWTP.

3.1.4. Digestion chambers and sludge buffer tank

The two digestion chambers were surveyed for leaks on two measurement days using the cold sky as background to increase the temperature contrast, but no leaks were found from the digestion chambers at the WWTP.

An additional source of emissions was however the sludge buffer close to the digestion chambers, for which we measured emissions of 10.7 kg CH_4/d and 3.8 kg N_2O/d, based on one measurement day. The buffer tank has a variable level of sludge material, with a 0.1 m^2 hole in the top of the tank where gas flows out when material is added and air flows in when the level in the tank decreases. As we only made one hyperspectral measurement of this source and it is a very variable point source that can be measured using conventional techniques, we estimated yearly emissions using the average emission of three days based on the above mentioned hyperspectral and two additional conventional measurements (1.6 and 0.4 kg CH_4/d on 28 March and 14 August, respectively) giving yearly emissions of 1530 ± 1190 kg CH_4 and 550 ± 730 kg N_2O (assuming the same N_2O/CH_4 ratio as N_2O was not measured with the conventional method). The high uncertainties reflect the very high variability of this source between measurement days.

3.1.5. Sludge storage

At the plant there were always 12 piles used for sludge storage as the material is stored for a year (twice the required minimum time mentioned in Table 1), with a new pile replaced every month. During the first season we could not find any emissions from piles older than four months, and therefore focused on material up to 120 days old. In a typical measurement day where sludge deposits were targeted, we imaged piles representing the three or four most recent months, often combining several scenes and a corresponding visual CH_4 mosaic (Fig. 3). In total we measured emissions from 11 sludge piles over a year.

The sludge deposits were divided into four monthly categories based on their age (<30 d, 30–60 d, 60–90 d, and 90–120 d). Although there was a variability in the emissions across seasons (which in the category "< 30 d" was partly caused by some piles not being finished yet) a clear decrease in CH_4 emissions with time can be seen for all seasons, with very low relative emissions after four months (Fig. 4.).

Fitting an exponential decay function to the data (Fig. 4A) and considering that a typical sludge deposit at this plant increases in mass by 27 tonnes per day during until an age of 30 days we find the following relation for how emission per tonne dry sludge material changes with time:

$$F_w(t) = 125.57 \cdot e^{-0.025 \cdot t} \quad (1)$$

where F_w is the emission per weight sludge (kg CH_4/yr/tonne) and t the time passed from a sludge deposit was started until the time of measurement (days).

Fitting a polynomial to the measured emissions of the different sludge deposits versus their ages (Fig. 4B) with the condition of no emission at time 0 (because no pile had yet been created at time 0), we find the following relation for a typical pile at this particular plant:

$$F(t) = 0.399 \cdot t^3 - 77.276 \cdot t^2 + 3619.2 \cdot t \quad (2)$$

where F is the emission (kg CH_4/yr). The plotted curve (Fig. 4B) shows an increase in emissions from zero at the beginning of a pile as there is no material yet, reaching a maximum after 30 days when the pile is full, then decreasing with time.

For an average-sized pile, with a weight of 830 tonnes the total integrated yearly emission was found to be 6790 ± 1100 kg CH_4, giving a total lifetime (1 year) emission of 8.2 ± 1.3 kg CH_4 per tonne stored sludge. Uncertainty ranges for each sludge pile on the best-fit curves (Fig. 4) were estimated from the variability in emissions between the three measurement points (sludge piles) of each month. The total uncertainty in CH_4 emission was then calculated using a Monte Carlo simulation based on 1000 distributions of simulated measurement points, all located within the error bars shown in Fig. 4. From 1000 fitted curves and simulated total emissions, the standard deviation of these emissions represents the uncertainty in our best estimate.

As there are always 12 piles in the sludge storage area (one new started each month) this means a total yearly emission of 81 500 ± 3800 kg CH_4 which was by far the largest CH_4 emission source at the plant.

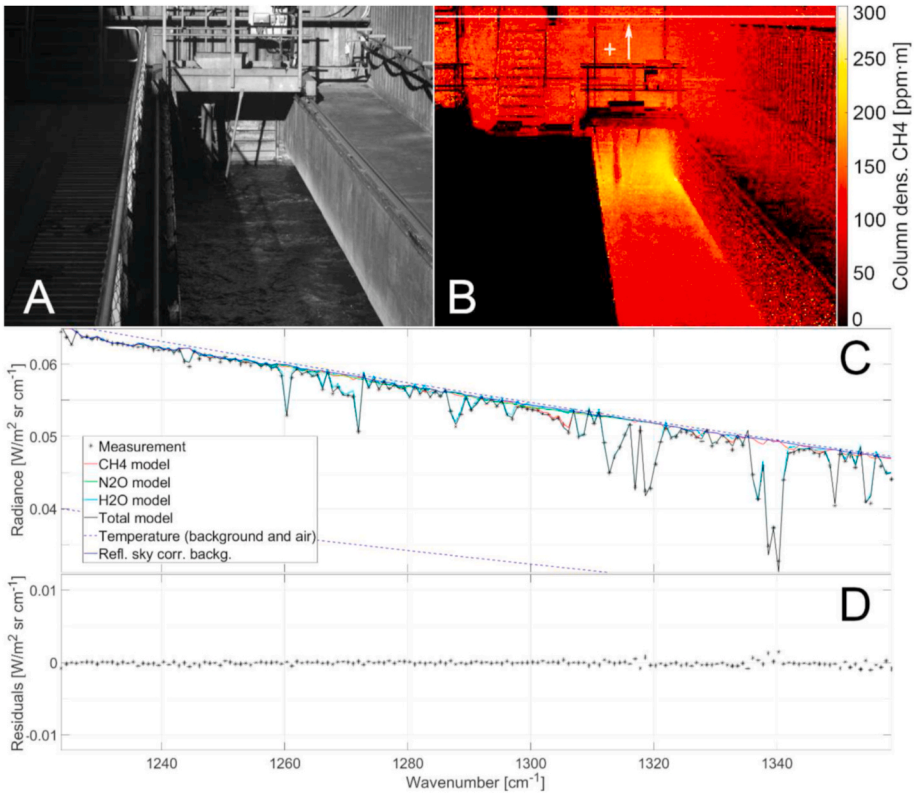

Fig. 2. The grit removal processing step with a monochromatic visual image (A), the calculated CH_4 distribution map (B), an example spectrum (C), and residuals of the spectroscopic model (D) for the pixel marked with a cross in panel B. The arrow indicates the air direction and the white line the horizontal area used for mass balance calculations to determine the emissions.

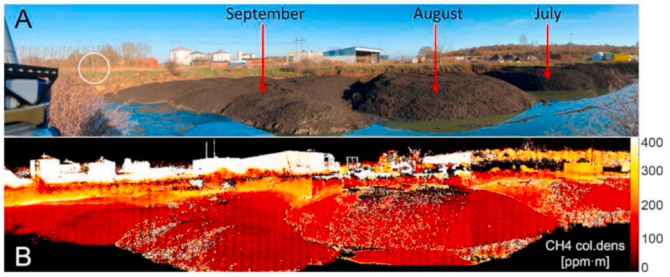

Fig. 3. Visual (A) and hyperspectral CH_4 mosaic (B) of three sludge deposits from measurements made November 12th, 2019, having ages of 2–4 months. A mobile weather station (marked with a circle) can be seen in panel A. Black pixels in the CH_4 mosaic are indicative of background-air temperature differences close to 0 (for which CH_4 column densities could not be calculated). There is an excess of CH_4 across the whole mosaic, with higher concentrations in the left part (youngest pile) and at locations in the scene with low wind speed (yellow features). (For interpretation of the references to colour in this figure legend, the reader is referred to the Web version of this article.)

The emissions correspond to about 6 % of the CH_4 produced during sludge digestion in the digestion chambers.

3.1.6. SHARON reactor

The SHARON reactor showed very variable emissions of N_2O ranging from 10 to 170 kg/d on a full cycle scale (Fig. 5). By calculating emissions from each data cube, giving a time resolution better than 1 min, a clear correspondence between fluxes for both CH_4 and N_2O and the operational aeration/non-aeration cycle of approximately 90 min could be reveled (Fig. 6). There was a "phase shift" of 180° between the two gases, i.e. CH_4 emissions peaked during the non-aeration period, while N_2O peaked during aeration. Given this extensive temporal variability

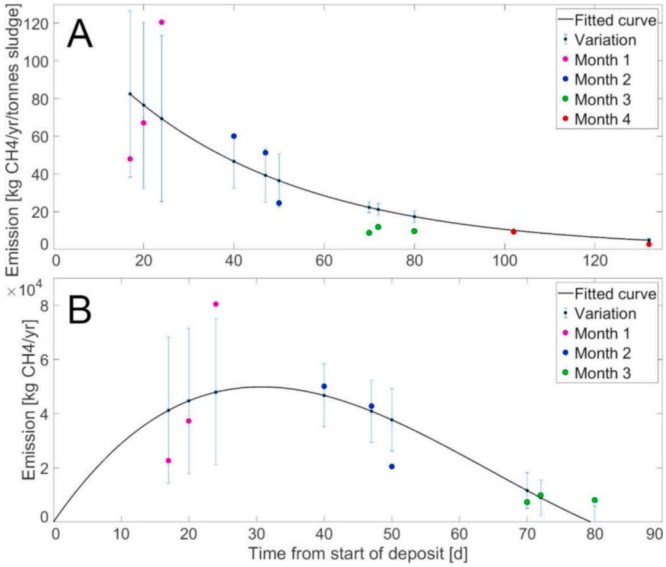

Fig. 4. Change in CH_4 emissions with sludge deposit age for all measured piles. The emission per tonne sludge (A) described by an exponential decay function, showing decreasing emission with time as the material gets older. The emission for a typical sludge pile at this particular plant (B) described by a 3rd deg. polynomial. Age is defined as the time from the start of a sludge deposit to the date of measurement. Emissions increase during the first 30 days as new material is added to the pile and thereafter decline over time. Error bars marks uncertainty intervals centered on the best fitted curves. See text for equations.

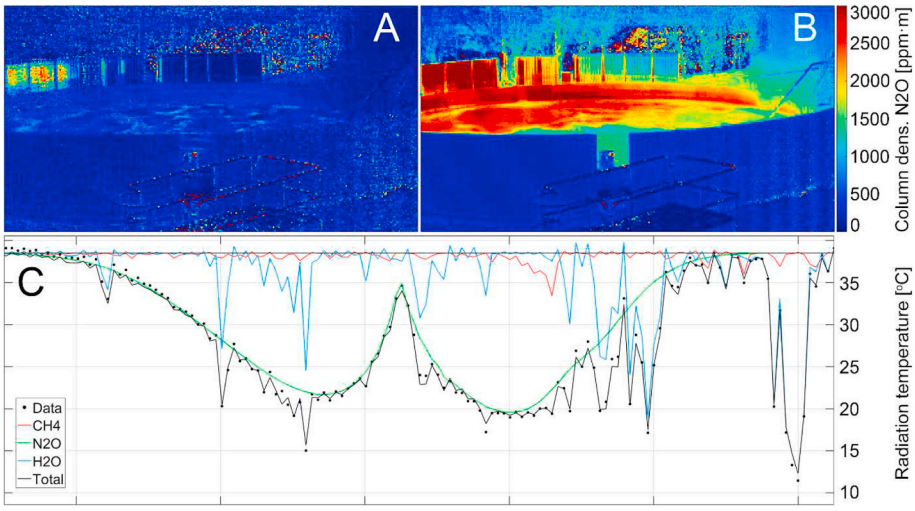

Fig. 5. N_2O maps of the SHARON treatment step for non-aeration (A) and aeration (B) periods and an example spectrum with fitted models of CH_4, N_2O, H_2O, and total absorption for a line of sight during high emissions (C).

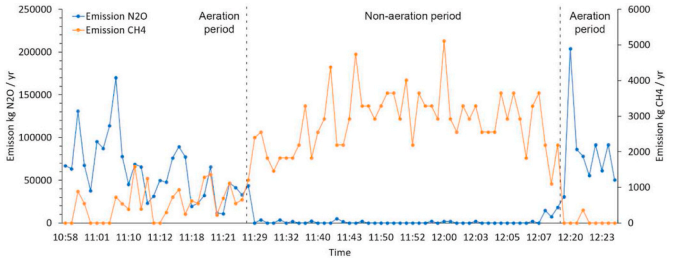

Fig. 6. The detailed variability in CH_4 and N_2O fluxes during one complete cycle of the SHARON reactor, showing much higher N_2O emission during the aeration period and higher CH_4 emission during the non-aeration period.

on a hourly basis, single short-term measurements could give very misleading information (Fig. 5), in this case in the range 0–550 kg N_2O/d and 0–13.7 kg CH_4/d on a minute timescale.

Following the CH_4 and N_2O fluxes from the SHARON reactor for at least one operational cycle on all six measurement days during a year and correlating this with parameters from the on-line monitoring indicative of conditions for high and low N_2O emissions, a yearly emission could be calculated.

Considering information from on-line monitoring of parameters in the tank, high levels of nitrite and ammonium coincided with high N_2O emissions to air (data not shown). Dividing a full year of continuous nitrite and ammonium data into time periods corresponding to conditions for low and high N_2O emission it was found that 90 % and 10 % of the time had potential for low and high N_2O emission, respectively. From the hyperspectral data we calculated the yearly emissions of 4700 ± 760 kg N_2O/yr and 54 200 ± 7020 kg N_2O/yr for these two classes. These assumptions yielded a total estimated emission for a year of 9700 ± 980 kg N_2O (equivalent in 100-year warming potential to 2 900 000 kg CO_2).

Our CH_4 measurements showed lower emissions during the aeration period, which is logical given the likelihood of rapid degassing of the CH_4 right upon start of aeration and limited new production and/or possibly CH_4 oxidation in the presence of O_2. However, some CH_4 emission occurred during aeration (Fig. 6) possibly due to CH_4 coming with the inlet water from the upstream treatment step (drying of sludge in anaerobic conditions). The high CH_4 fluxes during the non-aeration period were likely sustained by both incoming CH_4 and production in the tank when O_2 was depleted. A possibility for this CH_4 production is that the microbial community, added to the tank from the previous treatment step, can use the external carbon source (ethanol) added in the beginning of the non-aeration phase, and on-line monitoring data showed that the highest CH_4 flux coincided with the highest dosage of ethanol. During a full year, we estimate that high doses of ethanol were added 10 % of the time (based on the duration of high pH). Dividing the year into two cases; 90 % with low potential for CH_4 emissions (1610 ± 560 kg CH_4/yr) and 10 % with high potential for CH_4 emissions (11 690 kg CH_4/yr) the estimated total yearly emission was found to be 2620 ± 500 kg CH_4 (equivalent in 100-year warming potential to 89 000 kg CO_2).

3.1.7. Biological treatment

The biological treatment is carried out in three different areas of the plant, each with a basin that has phases of aeration and non-aeration, for which we measured over a cycle each measurement day focusing on the biological treatment. Our first measurement (autumn 2018) did not show any emissions in either of the phases. In the following measurements we chose to focus on one of the basins (the rightmost in Fig. 1) that had a sunlit brick wall as a background. The thermal contrast was increased even more on parts of the well using a Halogen lamp to heat it up.

Using measurements from nine days in the ranges 0–9 kg CH_4/d and 0–2.7 kg N_2O/d, each including a full cycle, yearly emissions of 640 ± 400 kg CH_4 and 260 ± 140 kg N_2O were calculated. The emissions varied between the different measurement days indicating some process variability, however, flux levels were overall small compared to the total emissions of the WWTP.

3.1.8. Drug residue, N removal, and secondary clarifier steps

No emissions were found from these treatment steps when measured on two days with high thermal contrast. This indicates that these treatment steps have negligible CH_4 or N_2O emissions relative to their areas, passing air masses and compared to other flux sources at the WWTP.

3.1.9. Incomplete flaring of methane at the wastewater treatment plant

During our measurements downwind of a ventilation outlet (Fig. 7) there was a very sudden and extreme increase in CH_4 concentrations. This was due to a flaring event with incomplete burning of excess CH_4 gas some distance behind and upwind of our target area. The imaged plume showed column densities in excess of 300 000 ppm m between the camera and the building in the background (12–20 m distant), corresponding to average CH_4 concentrations of up to 25 000 ppm (2.5 %). As part of another project, the same ventilation outlet was measured the

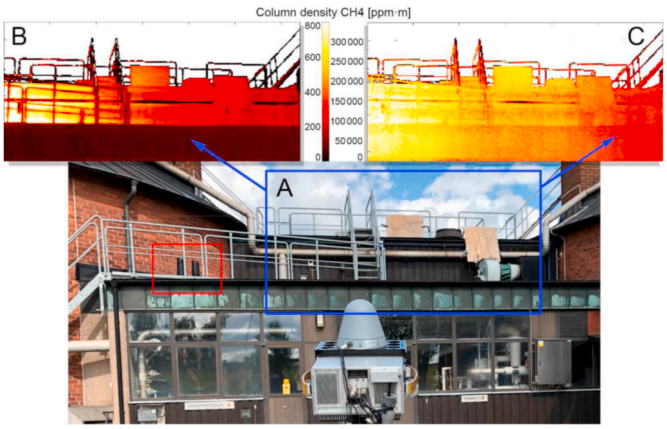

Fig. 7. Visualization of the unexpected incomplete flaring of excess CH_4 at the plant during measurements of a ventilation outlet. The visual image (A) shows the ventilation outlet (red square) and camera field of view (blue square) downwind of the outlet, with CH_4 column density maps before (B) and during the flaring event (C). The flaring took place behind the camera with winds blowing the plume into the field of view at times with southerly winds. Note the elevated CH_4 levels in panel C. (For interpretation of the references to colour in this figure legend, the reader is referred to the Web version of this article.)

same day using a traditional method based on air speed and gas concentration measurements inside the ventilation pipe, which does not enable detection of the flaring event and resulting CH_4 concentrations, showing the advantages of remote sensing to pick up unexpected emissions.

Although probably only part of the plume entered our field of view, a conservative emission estimate based only on the CH_4 in our field of view gave a flux of at least 30 kg CH_4/min, corresponding to almost 200 times the total CH_4 emission of the entire WWTP during the duration of our measurements (unknown source duration as our target was not the flaring, however plumes periodically entered our field of view during the 2 h of measurements at this measurement location). Compared to the timescale of a year, events of incomplete CH_4 flaring are probably rare and of short duration, however, given the extremely high fluxes involved, and the inability of conventional methods used for routine controls to capture such fluxes, future studies would be of interest for investigating the contribution from this source type, accounting for frequency, durations, and typical emissions. If our estimate is correct, such emissions from incomplete flaring for only two days per year would double the total yearly emission from the plant.

Table 3
Summary of yearly emissions from each treatment step and from the overall plant. See Table 2 for explanations of abbreviations and text for details.

Process step	CH_4 emissions (kg/yr) (Nm^3/yr)		N_2O emissions (kg/yr) (Nm^3/yr)	
Grit removal	3 160 (4660)	±1 250 (1840)	360 (190)	±330 (180)
Aeration	960 (1420)	±290 (430)	bd	
Sludge buffer	1 530 (2260)	±1 190 (1760)	550 (290)	±730 (390)
Sludge storage	81 500 (120 200)	±3 800 (5600)	bd	
SHARON reactor	2 620 (3860)	±500 (740)	9 700 (5180)	±980 (520)
Biological	640 (940)	±400 (590)	260 (140)	±140 (75)
Flaring events[a]	43 200 per event-day	–	bd	
Total[b]	90 400 (133 300)	±4 240 (6 250)	10 870 (5800)	±1 280 (680)
Total CO_2eq (100 yr)[b]	2 260 000 (1 226 900)	±110 000 (59 700)	3 200 000 (1 737 000)	±390 000 (211 700)

[a] Value for a total time of emissions corresponding to 1 day per year is provided for comparison. The total time of emission per year for this emission type in not known.
[b] Flaring events not included making this value conservative.

Table 2
Summary of all the treatment steps at the WWTP from the hyperspectral data. The range in age of sludge deposits are referring to the average storage time of the material in each pile. Measurements with no detected emissions are marked by bd (below detection; can be due to low fluxes and/or poor measurement conditions with too low temperature contrast). Process steps measured more than once in a given time period are indicated by 1st-3rd meas., and steps without measurements in that time period are marked with a – sign.

Treatment step	Fall 2018		Spring 2019		Summer 2019		Fall 2019	
	CH_4 (kg/d)	N_2O (kg/d)	CH_4 (kg/d)	N_2O (kg/d)	CH_4 (kg/d)	N_2O (kg/d)	CH_4 (kg/d)	N_2O (kg/d)
Grit removal	3.7	bd	2.4	3.7	11.5	<0.3	17	bd
Aeration	4.2	bd	1.5	bd	2.2	Bd	–	–
Primary clarifier	bd[b]	bd[b]	bd	bd	bd	Bd	–	–
Digestion chamb.	bd[b]	bd[b]	bd	bd	bd	Bd	–	–
Sludge buffer	–	–	10.7	3.8	–	–	–	–
Sludge storage								
<30 d	220	bd	102	bd	62	Bd	–	–
30–60 d	–	–	56	bd	117	Bd	137	bd
60–90 d	27	bd	22	bd	–	–	20	bd
90–120 d	21	bd	–	–	–	–	–	–
120–150 d	<6	bd	–	–	–	–	–	–
SHARON[a]								
1st meas.	5.2	165	9	110	<1	10	<1	17
2nd meas.	32	12	6	170	–	–	–	–
Biological[c]								
1st meas.	Bd	bd	9	2	2	2.7	3	<1
2nd meas.	Bd	bd	–	–	bd[b]	bd[b]	bd	bd
3rd meas.	–	–	–	–	2	1.5	–	–
Drug residue	bd[b]	bd[b]	–	–	–	–	–	–
N removal MBBR	bd[b]	bd[b]	–	–	–	–	–	–
Second. clarifier	bd[b]	bd[b]	–	–	–	–	–	–
Flaring event[d]	–	–	–	–	>30[d] kg/min	Bd	–	–

[a] Emissions are averages of the full 90 min cycle of the SHARON.
[b] Several measurements were made during the time period.
[c] Emissions are averages of the aerated on non-aerated periods of the biological treatment.
[d] Please note the separate unit for this flux, being rare and episodic, making estimates for extended time periods challenging. The value given regards an estimate from one event unexpectedly discovered (see text for details).

3.1.10. Total CH_4 and N_2O emissions from all treatment steps

By combining all the emissions detected by the hyperspectral measurements (Table 2) we estimated the total CH_4 and N_2O emissions at the WWTP (see Table 3).

The total CH_4 emission previously measured from the plant with traditional methods was only 3350 kg CH_4/yr, much lower than the 90 400 kg CH_4/yr from remote sensing in our study (corresponding to 6.7 % of the biogas production from sludge digestion at the plant). The reason for this is that many important emission sources belong to treatment steps that are extended sources, mainly sludge storage, which is presently not included in routine measurements, instead focusing mainly on ventilation outlets and specific potential leak points. This study highlights the need for methods that can quantify all types of emissions sources, including distributed non-point sources (which clearly dominated over point sources) and at the same time having the ability to scan scenes and discover unknown sources that may be of importance.

3.1.11. Measures to reduce GHG emissions

We have identified sludge deposits as the dominant source of GHG emissions at both the Linköping and at nearby Norrköping WWTP. These emissions arise due to organic material, remaining microorganisms from the digestion chambers, and a favorable environment for CH_4 production. The organic material can be influenced by changing the efficacy of the digestion process. It should also be possible to reduce emissions from the storage piles by modifying the environment, making it less favorable for the microorganisms, this could for example be a reduction of the sludge temperature or by adding substances such as ammoniacal nitrogen (Fidjeland et al., 2013; Willén et al., 2016) or an increased oxygen supply. Another possibility would be to collect the produced gas for incineration, preferably using the generated heat for other purposes.

The dominant source for N_2O emissions was the nitrogen removal of reject water, being quite rich in ammonia (Massara et al., 2017), which at the Linköping plant is the SHARON reactor, having variable emissions that could sometimes be very high. Changing the reactor technique to another type, e.g. a DeAmmon reactor would reduce the emissions substantially (we did test measurements at the Norrköping plant which uses a DeAmmon reactor and found no N_2O emissions). Optimizing the operation of a SHARON reactor can also lower emissions which is suggested by our measurements, as there is a correlation between high nitrogen content in the reject water and high N_2O emissions (Baresel et al., 2016) which we also found in our study.

3.2. Comparisons with other WTTPs

3.2.1. Comparison with other full-scale studied in literature

Normalizing our full-scale WWTP CH_4 emission to emission per person and per m^3 influent wastewater (Table 4) we find that the Linköping WWTP had relatively low emissions. In this comparison, we have not included sludge storage as this source is not included in the other studies. We however note that sludge storage corresponds to 90 % of the total CH_4 emission at the plant, and that inclusion of this source would increase the normalized emissions considerably for all WWTPs that have sludge storage. A large increase could also come from flaring events and although we identify this is a potentially large emissions source, it is not possible from current data to estimate the duration and frequency of flaring events on the timescale of a year. Overall, it is vital to assess all large emission sources at WWTPs to enable meaningful comparisons of total WWTP emissions, and there is a risk that WWTP emissions globally have been grossly underestimated given the incomplete previous emission assessments.

Table 4
Comparison of normalized CH_4 emissions between our study and other full-scale studies in literature of WWTPs.

Study	g CH_4 person^{-1} yr^{-1}	g CH_4 (m^3 influent)$^{-1}$
Czepiel et al. (1993) - Durnham WWTP	39	0.14
Wang et al. (2011) - Jinan WWTP	11	0.16
STOWA (2010) – Papendrecht	266	2.44
STOWA (2010) – Kortenoord	140	1.56
STOWA (2010) - Kralingseveer (October)	310	2.73
STOWA (2010) - Kralingseveer (February)	230	2.03
Daelman et al. (2012) – Kralingseveer WWTP	306	3.44
This study[a]	61	0.58

[a] We do not include sludge storage in our estimates as this is not included in other studies in the comparison.

3.2.2. Comparison of sludge storage emissions with another WWTP in Sweden

As the dominating CH_4 source in the Linköping WWTP was sludge storage, we made additional measurements of sludge storage emissions at another WWTP in Norrköping (a nearby city with approximately 100 000 inhabitants; located 39 km from Linköping) as a comparison and to check if our results were valid also at other WWTPs. Measurements for the three youngest sludge piles were made from of distance of 120–200 m (Fig. 8) on Apr. 25, 2019, yielding a total flux of 137 kg CH_4/d. Follow-up measurements on Jun. 28, 2019 were made on individual sludge piles yielding fluxes of 200 kg CH_4/d (age 28 days), 56 kg CH_4/d (age 58 days) and 16 kg CH_4/d (and 88 days). The three piles have a total flux of 272 kg CH_4/d, which can be compared to the corresponding emission of 254 kg CH_4/d for three typical, equally aged piles at the Linköping WWTP (Table 2). These results confirm that sludge storage is the dominating CH_4 source for two large WTTPs in Sweden and that the emissions are of similar magnitude between the plants, with a similar dependence on sludge age.

3.3. Biogas plant

The biogas plant is located north of the WWTP and is connected via a

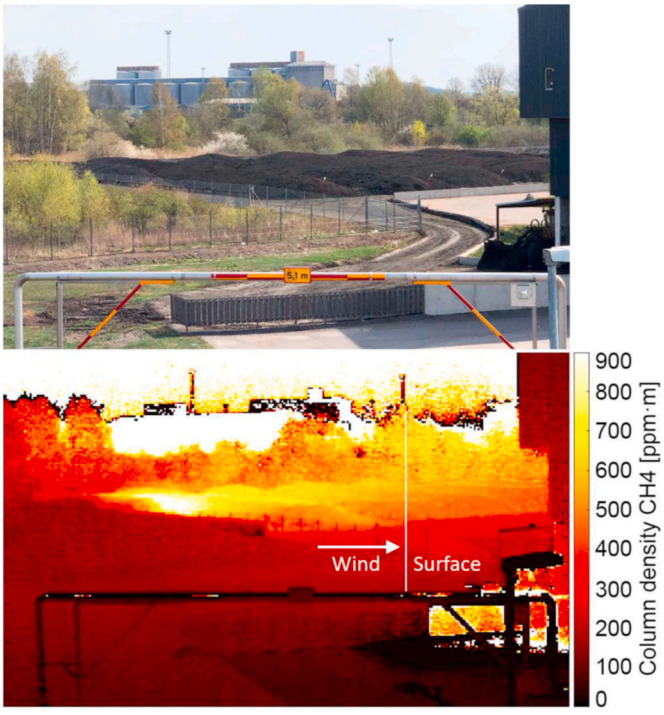

Fig. 8. Visual image (A) and calculated CH_4 map (B) for the sludge storage at the Norrköping WWTP. The line marks the vertical surface used to calculate the total CH_4 emission from the three youngest sludge piles (left in the image).

gas pipeline transporting gas from the WWTP digestion chambers to almost pure CH_4. It also has its own digestion chambers, producing biogas from organic material such as food and slaughterhouse waste (total production of 22 800 kg CH_4/d). A known source of CH_4 emissions prior to his project was the tank where biofertilizer material is stored. This source and two previously unknown sources are described and discussed in separate sections below.

3.3.1. Biofertilizer storage tank

We measured this source in a separate effort described in detail elsewhere (Gålfalk et al.; in review) and found a total emission of 144 ± 32 kg CH_4/d (52 600 ± 11 700 kg CH_4/yr). The measurements were made on the September 5, 2018 and included the whole tank with a diameter of 37.5 m (surface area 1104 m^2 and maximum storage volume of 4000 m^3). Air motion on the downwind side of the circular tank was calculated from interference-corrected differential IR images of the hyperspectral camera and obtaining the total emission through a vertical area at the edge of the tank with calculated CH_4 column densities.

3.3.2. The unexpected discovery of a biogas production plant leak

While mapping CH_4 emissions from sludge deposits (extending 18–50 m from the camera setup; e.g. Fig. 3) we discovered an unknown high emission source which was identified as a leak in the adjacent biogas plant situated at a distance of 250 m from the camera. After calculating new transmission models for CH_4 at these higher absorption levels we made a map of the CH_4 column density distribution (Fig. 9). Using an interference corrected IR difference video (Supplementary data) it was then possible to calculate horizontal and vertical plume velocities (Fig. 10). From mass balance modeling we obtained the total flux of the leak after integrating fluxes along a horizontal and vertical surface area (Fig. 9).

The total flux was calculated to be 245 ± 34 kg CH_4/d (89 500 ± 12 500 kg CH_4/yr), corresponding to 1.1 % of the CH_4 produced by the biogas plant. After the discovery of this leak it was sealed. Going back to a set of test measurements made one year earlier (from another measurement spot) we found this leak in the older data as well from a large distance, having a similar emissions rate. This shows that high emission

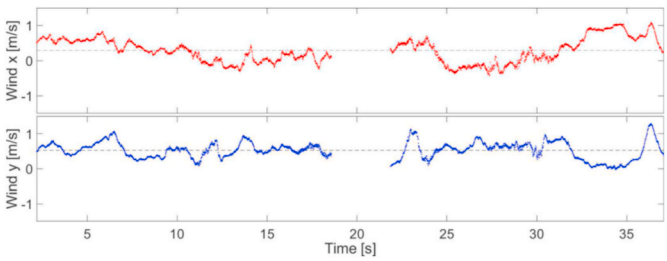

Fig. 10. Tracking of horizontal (x) and vertical (y) air motion in the plume from the biogas plant, with average values used in the mass balance calculations represented the dashed lines.

leaks can go undetected in routine inspections as they may be located in places that are difficult to reach or to survey from a close distance, as well as not being part of regular routine measurement spots. We also note that the leak is of similar magnitude as the total CH_4 emission of the whole adjacent WWTP. This example also shows that once detected, such leaks can rapidly and effectively be remedied, highlighting the benefit of effective measurement methods.

3.3.3. Emissions from loading of organic material onto trucks

From the set of measurements targeting the left side of the biofertilizer storage tank we found that during the event of a truck being filled up with biofertilizer material, this becomes an additional unexpected emission source (Fig. 11) with a flux of 74.4 kg CH_4/d which is about half that of the entire storage tank flux during the specific leading period.

Although this source may not be important on the timescale of a year (if trucks are not that frequent) it shows the importance of accurate source identification, including the discovery of unexpected emissions, to ensure representative flux estimation on longer timescale based on measurements made on shorter timescales.

3.3.4. Combined emissions at the biogas plant

Combining the sources (biofertilizer storage tank, big gas leak, and

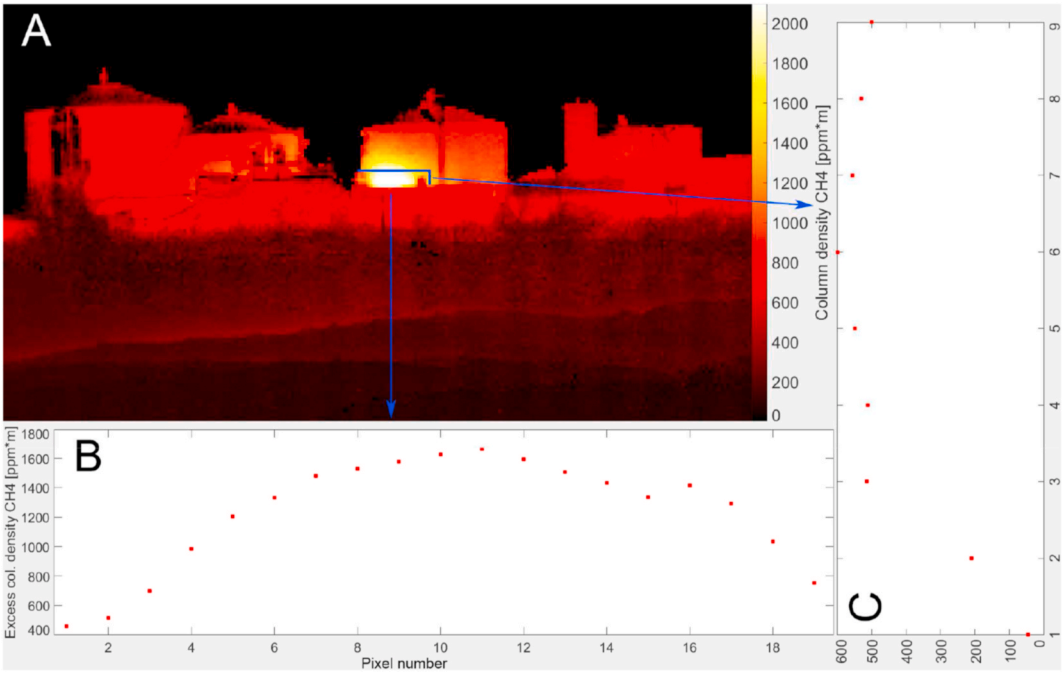

Fig. 9. Emissions of CH_4 from a leak at the adjacent biogas plant (250 m distant). A calculated CH_4 column density map (A) is combined with vertical (B) and horizontal (C) flux profiles to give an estimate of the total flux via mass balance calculations. The x- and y-axes in B and C represent pixel number along the horizontal and vertical lines respectively and the excess column density (beyond the background) in ppm·m.

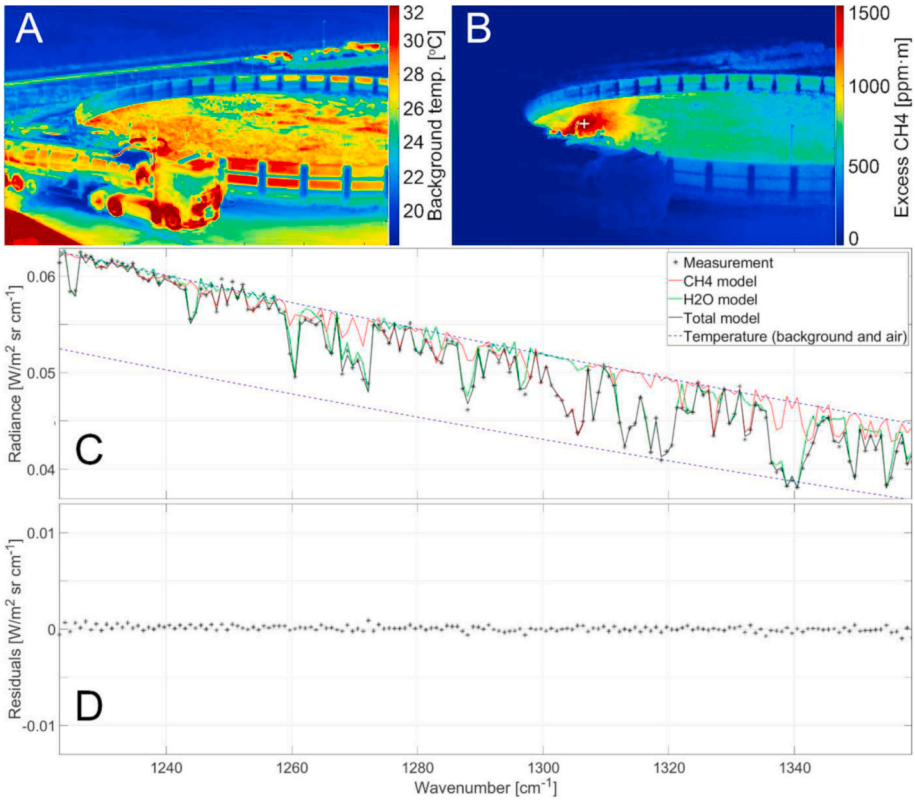

Fig. 11. Background temperature (A) and excess CH_4 map (B) of truck loading biofertilizer material from a storage tank at the biogas plant. Spectroscopic modeling (C) with residuals (D) for an example spectrum at the position marked with a white cross in panel B.

trucks filling up with biofertilizer) we found an overall emission from the biogas plant in the range 52 600–170 000 kg CH_4/yr (0.6–2.1 % of the CH_4 produced) depending on if the previously unknown sources (loading of trucks and leakage) are included or not (at times these make up almost 70 % of the total emissions). This represents a crude estimate which is less comprehensive than for the WWTP and a more systematic effort would be needed for assessing total biogas plant emissions at greater accuracy.

4. Conclusions

This study, representing one of the first attempts to assess total CH_4 and N_2O fluxes from a WWTP and adjacent relevant facilities using novel ground-based remote sensing, reveals that previous efforts with traditional methods grossly underestimate total fluxes. In our case, 90 % of the total continuous fluxes were previously undetected. On top of this there were several unexpected and very high episodic fluxes, potentially more than doubling overall emissions, that were not known previously at that require additional work for accurate long-term quantification. This study thereby highlights that it is absolutely essential to have effective methods for measurements of all types of greenhouse gas fluxes and for effective detection of unknown episodic emission sources to allow making adequate priorities and design effective actions to mitigate the emissions. Ground-based remote sensing is shown by this study to be a highly capable approach to meet these needs for improved greenhouse gas flux measurements at WWTPs, biogas plants and other relevant facilities.

Supplementary data related to this article can be found at https://doi.org/10.1016/j.envres.2021.111978.

Declaration of competing interest

The authors declare the following financial interests/personal relationships which may be considered as potential competing interests: Authors Sören Nilsson Påledal and Robert Sehlén work at the wastewater treatment plant and gave us access to the plant form doing measurements, as well as contributed with process descriptions of the treatment steps at the plant.

Acknowledgements

Funding: The work was supported by the Swedish Research Council VR (grant 2016-04829), Formas (grant 2018-01794), the European Union's Horizon 2020 research and innovation programme under grant agreement No 101015825 (TRIAGE) and an instrument grant from the Knut and Alice Wallenberg Foundation (ref no. KAW2010.0126). This project has received funding from the European Research Council (ERC) under the European Union's Horizon 2020 research and innovation programme (grant agreement No 725546). We are very grateful to Camilla Johansson at Tekniska Verken for valuable contributions throughout the project, and highly appreciate the assistance related to measurements from involved staff at Tekniska Verken and at Slottshagens wastewater treatment plant run by NODRA, Norrköping, and the field assistants from personnel at Tema Environmental Change, Linköping university.

Appendix ASupplementary data

Supplementary data to this article can be found online at https://doi.org/10.1016/j.envres.2021.111978.

References

Baresel, C., Andersson, S., Yang, J.J., Andersen, M.H., 2016. Comparison of nitrous oxide (N2O) emissions calculations at a Swedish wastewater treatment plant based on water concentrations versus off-gas concentrations. Adv. Clim. Change Res. 7 (3), 185–191. https://doi.org/10.1016/j.accre.2016.09.001.

Czepiel, P.M., Crill, P.M., Harriss, R.C., 1993. Methane emissions from municipal wastewater treatment processes. Environ. Sci. Technol. 27 (12), 2472–2477.
Bril, A, Oshchepkov, S, Yokota, T, Yoshida, Y, Morino, I, et al., 2013. Retrievals of atmospheric CO2, CH4 and optical path modifications from the GOSAT observations. Proc. SPIE, 8890:889008. https://doi.org/10.1117/12.2028486.
Chambers, A.K., Strosher, M., 2008. Direct measurement of fugitive emissions of hydrocarbons from a refinery. J. Air Waste Manag. Assoc. 58, 1047–1056. https://doi.org/10.3155/1047-3289.58.8.1047.
Daelman, M.R.J., van voorthuizen, E.M., van Dongen, U.G.J.M., Volcke, E.I.P., van Loosdrecht, M.C.M., 2012. Methane emission during municipal wastewater treatment. Water Res. 46 (11), 3657–3670. https://doi.org/10.1016/j.watres.2012.04.024.
Fidjeland, J., Magri, M.E., Jonsson, H., Albihn, A., Vinneras, B., 2013. The potential for self-sanitisation of faecal sludge by intrinsic ammonia. Water Res. 47 (16), 6014–6023. https://doi.org/10.1016/j.watres.2013.07.024.
Gålfalk, M., Bastviken, D., 2018. Remote sensing of methane and nitrous oxide fluxes from waste incineration. Waste Manag. 75, 319–326. https://doi.org/10.1016/j.wasman.2018.01.031.
Gålfalk, M., Olofsson, G., Bastviken, D., 2017. Approaches for hyperspectral remote flux quantification and visualization of GHGs in the environment. Remote Sens. Environ. 191, 81–94. https://doi.org/10.1016/j.rse.2017.01.012.
Gålfalk, M., Olofsson, G., Crill, P., Bastviken, D., 2016. Making methane visible. Nat. Clim. Chang 6, 426–430. https://doi.org/10.1038/nclimate2877.
Hofman, J., Hofman-Caris, R., Nederlof, M., Frijns, J., van Loosdrecht, M., 2011. Water and energy as inseparable twins for sustainable solutions. Water Sci. Technol. 63 (1), 88–92.
IPCC, 2007. In: Pachauri, R.K., Reisinger, A. (Eds.), Core Writing Team, Climate Change 2007: Synthesis Report. Contribution of Working Groups I, II and III to the Fourth Assessment Report of the Intergovernmental Panel on Climate Change. IPCC, Geneva, Switzerland.
Jervis, D., McKeever, J., Durak, B.O.A., Sloan, J.J., et al., 2021. The GHGSat-D imaging spectrometer, Atmos. Meas. Tech. 14, 2127–2140. https://doi.org/10.5194/amt-14-2127-2021.
Massara, T.M., Malamis, S., Guisasola, A., et al., 2017. A review on nitrous oxide (N2O) emissions during biological nutrient removal from municipal wastewater and sludge reject water. Sci. Total Environ. 596, 106–123. https://doi.org/10.1016/j.scitotenv.2017.03.191.
Myhre, G., Shindell, D., Bréon, F.-M., et al., 2013. Anthropogenic and natural radiative forcing. In: Stocker, T., Qin, D., Plattner, G.-K., Tignor, M., Allen, S., Boschung, J., Nauels, A., Xia, Y., Bex, V., Midgley, P. (Eds.), Climate Change 2013: the Physical Science Basis. Contribution of Working Group I to the Fifth Assessment Report of the Intergovernmental Panel on Climate Change. Cambridge University Press, Cambridge, United Kingdom and New York, NY, USA.
Saunois, M., Stavert, A.R., Poulter, B., et al., 2020. The global methane budget 2000-2017. Earth Syst. Sci. Data 12, 1561–1623. https://doi.org/10.5194/essd-12-1561-2020.
Scheutz, C., Fredenslund, A.M., 2019. Total methane emission rates and losses from 23 biogas plants. Waste Manag. 97, 38–46. https://doi.org/10.1016/j.wasman.2019.07.029.
STOWA, 2010. Emissies van broeikasgassen van RWZI's. Amersfoort, the Netherlands.
Staebell, C., Sun, K., Samra, J., Franklin, J., Miller, C.C., et al., 2021. Spectral calibration of the MethaneAIR instrument. Atmos. Meas.Tech. 14 (5), 3737–3753. https://doi.org/10.5194/amt-14-3737-2021.
Thorpe, A.K., Frankenberg, C., Aubrey, A.D., et al., 2016. Mapping methane concentrations from a controlled release experiment using the next generation airborne visible/infrared imaging spectrometer (AVIRIS-NG). Remote Sens. Environ. 179, 104–115. https://doi.org/10.1016/j.rse.2016.03.032.
Tumendelger, A., Alshboul, Z., Lorke, A., 2019. Methane and nitrous oxide emission from different treatment units of municipal wastewater treatment plants in Southwest Germany. PloS One 14 (1), e0209763. https://doi.org/10.1371/journal.pone.0209763.
Wang, J., Zhang, J., Xie, H., Qi, P., Ren, Y., Hu, Z., 2011. Methane emissions from a full-scale A/A/O wastewater treatment plant. Bioresour. Technol. 102 (9), 5479–5485.
Willén, A., Rodhe, L., Pell, M., Jönsson, H., 2016. Nitrous oxide and methane emissions during storage of dewatered digested sewage sludge. J. Environ. Manag. 184, 560–568. https://doi.org/10.1016/j.jenvman.2016.10.025.